Tunnelling and Underground Space Technology 77 (2018) 249–260

Contents lists available at ScienceDirect

Tunnelling and Underground Space Technology

journal homepage: www.elsevier.com/locate/tust

Geotechnical characterisation of a weak sedimentary rock mass at CERN, Geneva

Elliot James Fern[a,*], Vanessa Di Murro[b,d], Kenichi Soga[a], Zili Li[c], Luigi Scibile[d], John Andrew Osborne[d]

[a] University of California Berkeley, Dep. of Civil and Environmental Engineering, Davis Hall, Berkeley, CA 94720, USA
[b] University of Cambridge, Dep. of Engineering, Trumpington Street, Cambridge CB2 1PZ, UK
[c] University College Cork, Dep. of Civil, Structural and Environmental Engineering, College Road, Cork, Ireland
[d] European Council for Nuclear Research (CERN), Site Management and Buildings Department, Route de Meyrin 385, 1217 Meyrin, Switzerland

ARTICLE INFO

Keywords:
Geotechnical characterisation
Molasse
Sandstone
Marl
Tunnelling
CERN

ABSTRACT

The European Organisation for Nuclear Research (CERN) in Geneva has extensive underground facilities, which were built over the past 70 years in a weak layered sedimentary rock called the *red molasse*. CERN has thus been continuously exploring its underground space and has gathered extensive geotechnical data from both laboratory and field tests. The data shows that the *red molasse* is composed of marls and sandstones forming 6 different geotechnical units with different geotechnical characteristics. The strength-stiffness relationship of the *red molasse* is lower than other molasses from other regions, and that the marls are significantly more ductile than the sandstones. Moreover, the intermediate rock units (sandy marls and marly sandstones) have similar strength but a different stiffness, a distinction which is not represented in the standard strength classification system. Although all rock units were subjected to the same diagenesis, one rock unit is found to be very weak with soil-like properties. A mineralogy analysis shows that this unit is composed of high plasticity clay, whilst the other marls units are composed of medium-high and low plasticity clay. The field tests show rapid and progressive transitions between the different rock units, which makes field prediction difficult. This paper presents an overview of the geotechnical data gathered by CERN as well as the geotechnical characterisation of the site The geotechnical characterisation presented in this paper also compares laboratory tests with field tests.

1. Introduction

Switzerland is composed of three distinct geological regions – the Alps, the Jura and the molassic plateau (Fig. 1). Whereas the Alps are predominately composed of strong sedimentary and crystalline rocks and the Jura of medium-strong limestones, the Swiss plateau is comprised of a weak to medium-strong sedimentary rock called molasse. Although the term *molasse* originates from the Switzerland, it is used for any orogenic deposits of similar genesis irrespective of their location (Hoek et al., 2005).

The *red molasse* at CERN is composed of sequential layers of marls and sandstones from the Miocene tertiary period and by the diagenesis of Alpine detritus in a soft water basin (Swiss Geological Survey, 2013). The sedimentation of the Alpine detritus, controlled by the geological activity, resulted in the formation of clay, silt and sand lenses with substantial spatial variation. This makes any site prediction very difficult. The molasse at CERN is around 300 m deep (CERN, 1972) and has an anisotropic stress field resulting from the tectonic thrust of the Alps. This paper presents the laboratory and field exploration of the *red molasse* and discusses its mechanical characteristics.

2. Brief history of CERN's underground facilities

CERN was founded in 1952 in Geneva, Switzerland, as a particle physics laboratory and the first particle accelerator was built in 1957 – the *Synchrocyclotron* (SC). It was only in 1976 that CERN went underground with the *Super Proton Synchrotron* (SPS), which is a 7-km-long circular tunnel at a depth of 40 m. Fig. 2 shows a schematic description of the underground facilities at CERN in which the smaller circular tunnel is the SPS tunnel. The machinery was housed in caverns and the access was provided by shafts. Since then, CERN has extended multiple times. In 1988, the *Large Electron-Positron Collider* (LEP) was built. It is a 27-km-long circular tunnel, making it the largest underground construction in Europe and one of Europe's longest tunnels at that time. Ten years later, The LEP was converted to the *Large Hydron Collider* (LHC) and additional caverns and access shafts were constructed,

* Corresponding author.
E-mail address: james.fern@berkeley.edu (E.J. Fern).

https://doi.org/10.1016/j.tust.2018.04.003
Received 5 November 2017; Received in revised form 14 March 2018; Accepted 3 April 2018
Available online 11 April 2018
0886-7798/

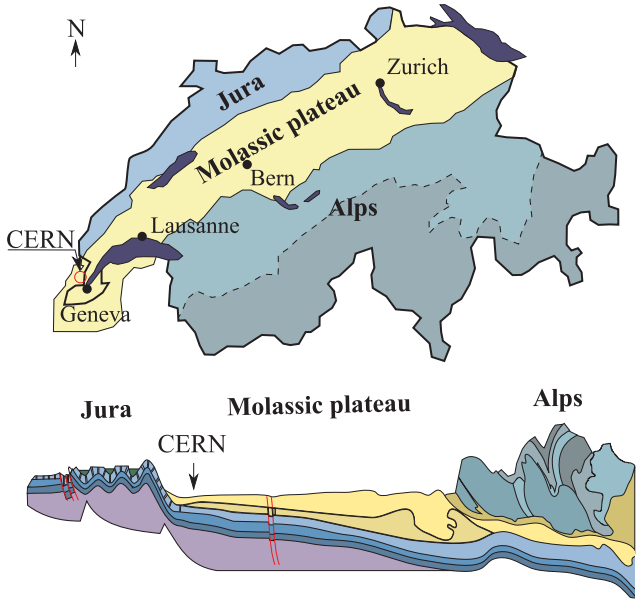

Fig. 1. Schematic description of the Swiss geology.

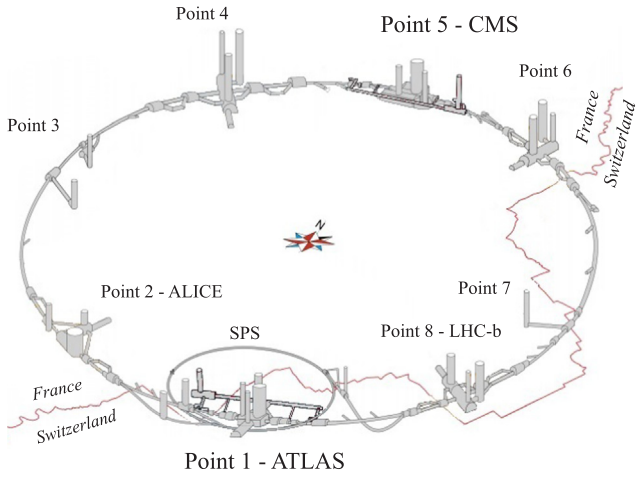

Fig. 2. Schematic description of the underground facilities at CERN.

including ATLAS (Point 1) and CMS (Point 5). Fig. 3 shows a photograph of the ATLAS cavern UX15 during construction, which is the largest cavern at CERN with excavated dimensions of L 55 × W 35 × H 40 metres. Shortly after, ALICE (Point 2) and LHCb (Point 8) were constructed adding new caverns and tunnels to the existing facilities. In 2015, the High Luminosity (HiLumi) project began with the construction of additional caverns, tunnels and shafts and will be operational by 2021.

3. Geotechnical exploration

The geotechnical investigations have been carried out for each new construction and were based on exploration boreholes from which samples were collected for laboratory testing. The boreholes were also used for site testing. The geotechnical characterisation presented in this paper is based on these investigations, and focusses on Point 1 (ATLAS) and Point 5 (CMS) since they offer the most extensive data as well as being at the two opposite positions of the CERN facilities. However, the geological conditions at Point 1 (ATLAS) and Point 5 (CMS) are slightly different. Point 1 (ATLAS) is located near Geneva airport where the bedrock roof is shallow (around 5 m) and Point 5 (CMS) is located next

Fig. 3. Excavation of the cavern UX15 at Point 1 (ATLAS).

to the Jura chain mountain where the bedrock roof is deeper (around 50 m). ATLAS was initially planned at Point 5 but was moved to Point 1 due to the more competent rock mass as it houses large caverns. The borehole logs show that the *red molasse* is primarily composed of layers of sandstone and marl with variable thickness. Fig. 4 shows an extract of the borehole C1 at Point 1 (ATLAS) and translated to English for this paper.

The term *sandstone* refers to cemented sandy or silty rocks and the term *marl* refers to clayey rocks. The borehole shows thick layers of sandstone separated by medium-thick, or even thin, layers of marl. However, thicker layers of marl are observed in other boreholes. This *red molasse* relates to 'Type III' molasse (Marinos et al., 2013) and it is characterised by systematic alternations of sandstone and marl of different grain-size grading with a thickness ranging from a few centimetres to a few metres, and few discontinuities. The *red molasse* is weak and fractured at shallow depths with rock quality designation *RQD* (Deere, 1963) values as low as 0. It is weathered and can have trenches at the surface (GADZ, 2016a), which are filled with quaternary fluvio-glacial soil units and are hazardous for tunnelling. The molasse is massive at depth with *RQD* values in the range of 70 to 100. The molasse can also contain some natural hydrocarbons GADZ (2016a), which affect the mechanical properties of discontinuities (Lombardi, 1979).

3.1. Rock units

Two types of rock are identified – marls and sandstone – and divided into 6 sub-units, 3 for each rock type. The description of these units is as follows.

The marls are micro-fissured rocks with various amounts of clay (40–60% of illite, 20–25% of chlorite), calcite and quartz (Fig. 5). They have smooth to slickensided closed and poorly-cemented joints with a spacing smaller than 60 mm. These marls are subjected to swelling, slaking upon contact with air and water, and spalling. According to the international rock classification (ISRM, 1981), the marls are very weak *R*1 to weak *R*2 rocks. Three sub-units were identified as follows.

- *1. Very weak marl* is mostly *motley* marl made from the diagenesis of high-plasticity clays (Figs. 5 and 6). It is characterised by numerous closed, polished, discontinuous and multi-directional micro-fissures, which give the rock isotropic characteristics. Its mineralogy gives it a low stiffness and ductile behaviour. This marl is subjected to swelling, slaking upon contact with air, and spalling.
- *2. Weak marl* is composed of *laminated* or *platty* marl and is composed of 45–60% of clay, 15–30% of micro-crystalline quartz, and 20–30% of calcareous minerals (Fig. 5). The Atterberg limits (Fig. 6)

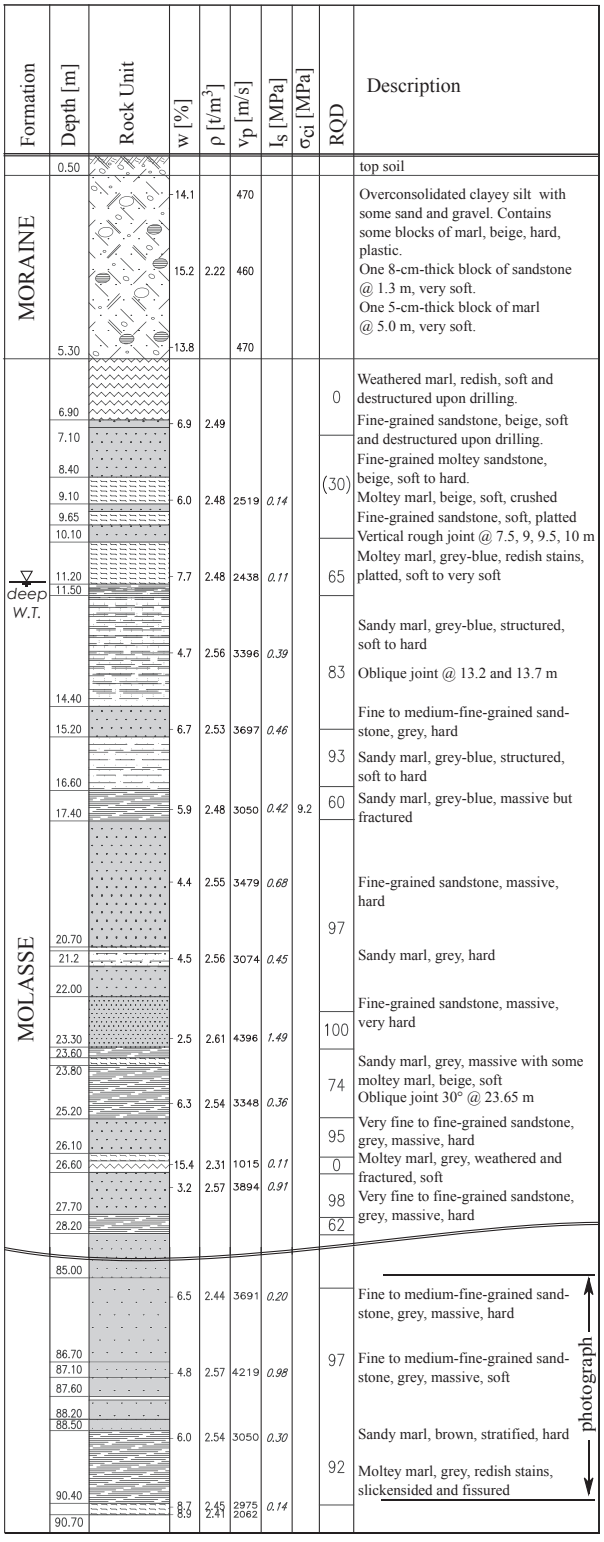

Fig. 4. Extract of borehole C1 log at Point 1 (ATLAS).

show that this rock unit is composed of medium-high plasticity clay, mostly illite but smectite and chlorite are also present. The micro-fissures are present but scares, and are mostly in a single direction inferring an anisotropic structure to the unit. The weak marl is also subjected to swelling, slaking upon contact with air, and spalling, albeit not as significantly as *1. very weak marl*.

– *3. Medium-weak marl* has similar proportion of clay (20–45%),

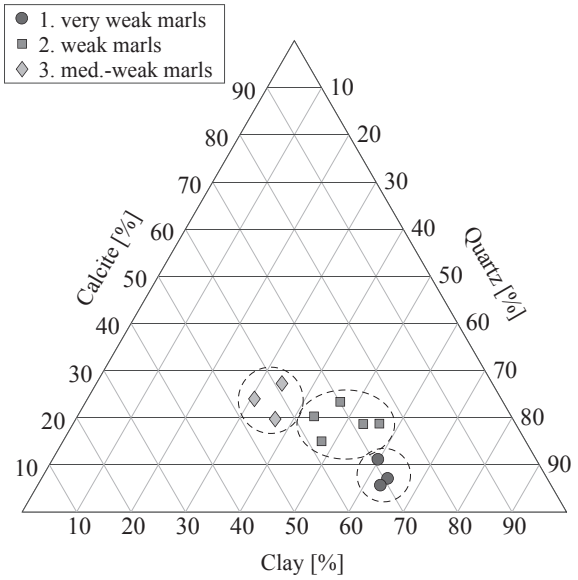

Fig. 5. Mineralogy of the marls.

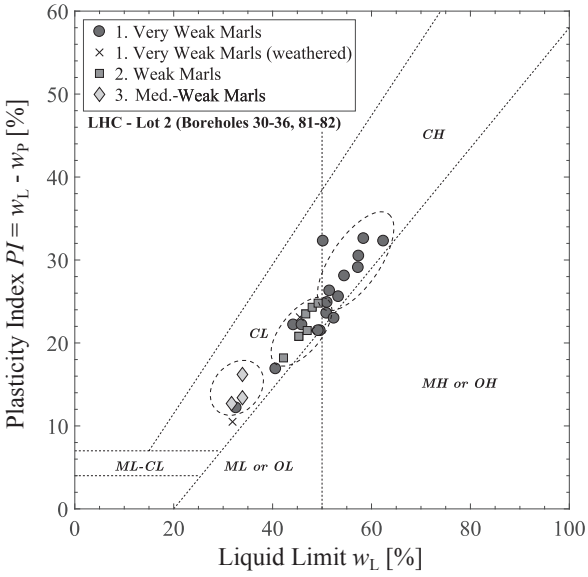

Fig. 6. Liquid limit and plasticity index of the marls.

quartz (20–40%) and calcite (20–30%) (Fig. 5). It is well cemented, which increases its strength and stiffness. The Atterberg limits (Fig. 6) shows that this rock unit was composed of low-plasticity clays. Although this rock unit is of type *R*2 weak rocks, it is referred to as 'medium-weak' because its mechanical characteristics are substantially better than those of *2. weak marl* and *4. weak sandstone*.

The sandstones are well-cemented silts and sands. The rock mass is homogeneous with a limited number of visible, rough and widely-spaced joints and the spacing is usually greater than 1 m. It is mainly composed of feldspar and silica but can contain some clay and calcite in variable amounts. According to the international rock classification (ISRM, 1981), the sandstones are mostly *R*2 weak to *R*3 medium-strong rock. Three sub-units were identified as follows.

– *4. Weak sandstone* is made of fine-grained poorly-cemented granular materials with some clay. It is weaker and softer than *3. medium-weak marls*, although it falls in the same rock category *R*2. It has 32% ± 1% of fines with a coefficient of uniformity of U_u = 11 and a

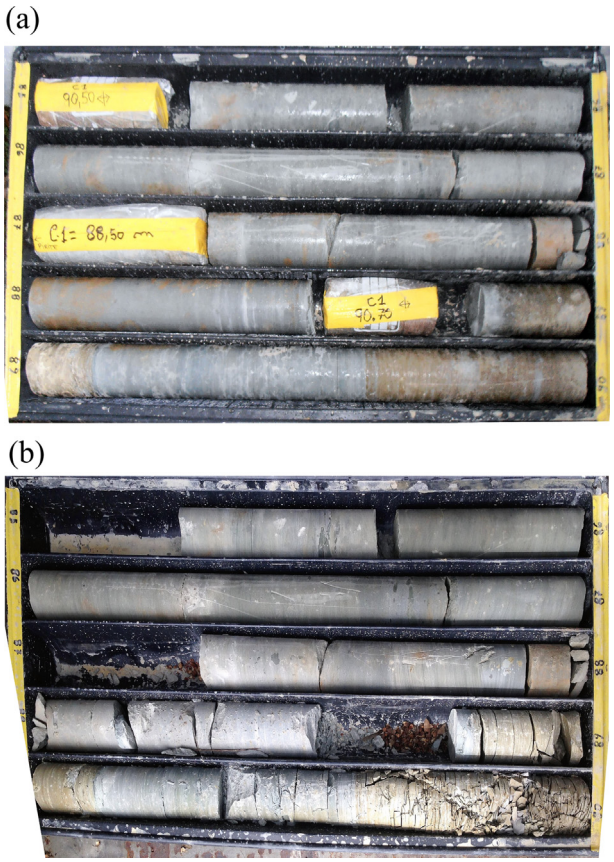

Fig. 7. Photograph of the core of borehole C1 at Point 1 at a depth of 85 m to 90 m: (a) after extraction (Oct. 2015) and (b) after 18 months storage (Mar. 2017).

coefficient of curvature of $U_c = 0.2$ with $D_{60} = 0.11$ mm (GADZ, 1997).

- *5. Medium-strong sandstone* is composed of well-cemented coarse-grained materials. It has good mechanical properties with rare discontinuities. It has 59% ± 7% of fines with a coefficient of uniformity of $U_u = 13$ and a coefficient of curvature of $U_c = 1.3$ with $D_{60} = 0.06$ mm (GADZ, 1997).
- *6. Strong sandstone* has a composition similar to *5. medium-strong sandstone* but better-cemented grains with fewer discontinuities, if any ($RQD \approx 100$). However, this rock unit is scarce. No grain-size analyses was available for *6. strong sandstones*.

Fig. 7(a) shows a photograph of a borehole core at Point 1 (ATLAS) at a depth of 85 to 90 m. The photograph shows red stain from which the *red molasse* was named. It also shows a smooth transition from one rock unit to another with very few discontinuities, although some drilling-induced disking occurred due to the higher stresses at this depth. The identification of each rock units can be difficult by visual inspection alone and laboratory testing is required. Fig. 7(b) shows the same core after 18 months storage in which the slaking of the *1. very weak marl* and *2. weak marl* is apparent at 90 m depth.

The classification of these rock units differed from one construction project to another. Some rock units were grouped together for design purposes. For instance, Lombardi (1979, 1981) suggested one class of marls for both *1. very weak* and *2. weak* marls, one class of intermediate rock for both *3. medium-fair marl* and *4. weak sandstone*, and one class of rock for both the *5. medium-strong* and *6. strong* sandstones. Sloan et al. (1996) followed the same approach for the design of the LEP/LHC tunnel but pointed out that the mechanical variation between sub-units of marls, sandstones and sandy marls. Laughton (1990) suggested using

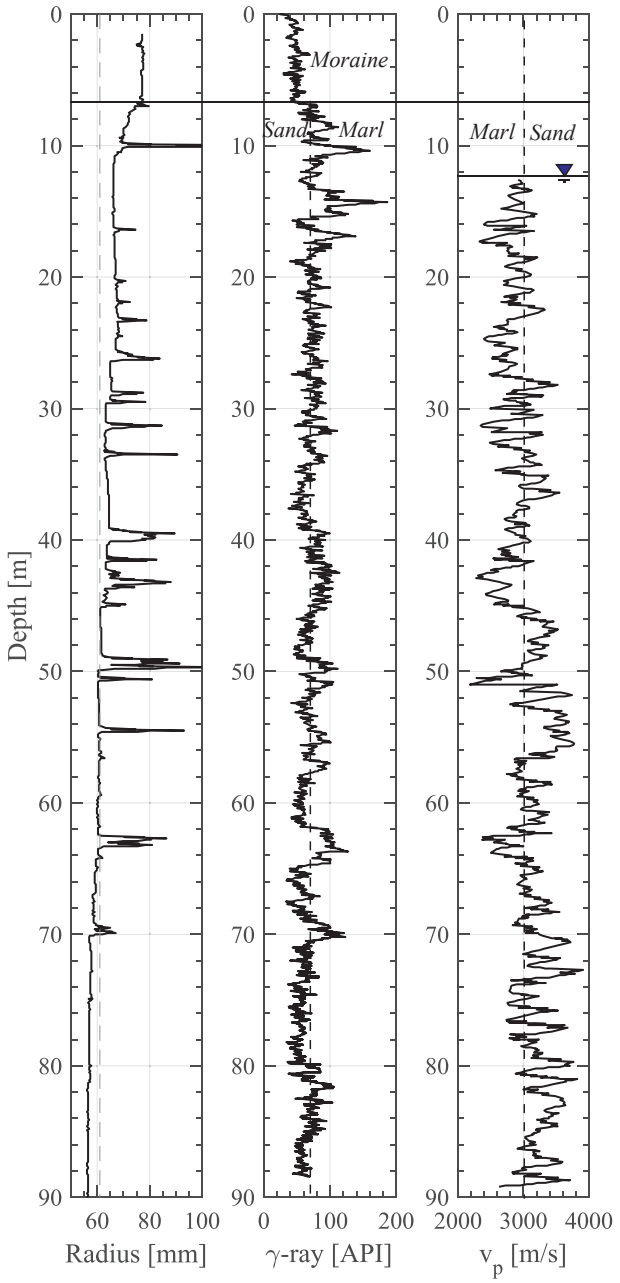

Fig. 8. Caliper, γ-ray and sonic wave velocity measurements in borehole C1 at Point 1 (ATLAS).

four groups – 2 for marls and 2 for sandstones. However, the soil-like characteristics of *1. very weak marl* encouraged GADZ (1997) to categorise it as a separate unit.

The interpretation of the borehole logs suggests a S-SW inclination of the bedding planes of 0° to 5° at Point 1 (ATLAS) (GADZ, 2016a) and Point 2 (ALICE) (Laughton, 1990), and 10° to 20° at Point 5 (CMS) (GADZ, 2016b). The difference in dip is due to the uplift of the Jura mountain chain.

3.2. Borehole exploration

A series of tests were carried out in the boreholes and the results of borehole C1 at Point 1 (Atlas) are presented in this section.

3.2.1. Caliper tests

Caliper tests were carried out and the results for borehole C1 Point 1

are given in Fig. 8. The test measures the diameter of the borehole and permits the detections of wall collapse. The results show that the walls collapsed systematically in *1. very weak marl* and *2. weak marl*, albeit not as extensively, and that it is a reliable means of detecting the presence of very weak rock.

3.2.2. γ-ray tests

Boreholes were scanned with γ-rays and the results for borehole C1 Point 1 are given in Fig. 8. γ-rays are absorbed in sand but are reflected back in clay. The results show that the rock mass with $API < 90$ is sandstone and $API > 90$ marl. They also show that the highest API values are reached in *1. very weak marl* and *2.weak marl* and the lowest in *5 medium-strong sandstone* and *6. strong sandstone*. Therefore, the intermediate values correspond to *3. medium-weak marl* and *4. weak sandstone*.

3.2.3. Sonic wave velocity

Sonic wave velocity tests were carried out in some boreholes and an example of results is given in Fig. 8. It can be seen that the marls have a P-wave velocity of $v_p = 2500–3000$ m/s and the sandstone of $v_p = 3000–3500$ m/s, which are in the range of the velocities measured on laboratory specimens. The velocity readings provide a means of differentiating *3. medium-weak marl* from *4. weak sandstone*, as the latter has a higher velocity. It is also possible to confirm the location of the stronger rock units – *5. medium-strong* and *6. strong* sandstones. However, the measurements were taken at depth intervals of approximately 50 cm, which does not permit an accurate determination of the rock units as their thickness is often smaller. This issue has been pointed out by Barton (2007).

3.2.4. Dilatometer tests

The *in situ* stress field is known to be anisotropic close to mountain ranges, with the major and intermediate stresses being horizontal and the minor being vertical (Heidbach et al., 2016). This is caused by the thrust of the Alps pushing the molassic plateau onto the Jura. Dilatometer tests carried out at a depth of 92 m confirmed the anisotropic stress field. The direction of the major principal stress was found to be oriented NE-SW with and the following earth pressure coefficients were calculated.

$$\text{Point 1:} \quad K_{0,max} = 2.00 \pm 0.3, \quad K_{0,min} = 1.50 \pm 0.1 \tag{1}$$

$$\text{Point 5:} \quad K_{0,max} = 1.75 \pm 0.5, \quad K_{0,min} = 1.29 \pm 0.1 \tag{2}$$

4. Element testing

Throughout the various projects at CERN, samples have been systematically collected from borehole cores, tested in different laboratories, and presented in the respective geotechnical interpretation reports. These samples were used to characterise the strength, stiffness and state. Statistical values were obtained by GADZ (2016a,b) and are summarised in Table 1. Variables with less than 5 tests are given in brackets but cannot be considered as statistically representative. The table gives the mean values for the entire CERN site.

The mean water content w (Table 1) decreased from 8.6% for *1. very weak marl* to 5.0% for *3. medium-weak marl*, and from 7.8% for *4. weak sandstone* to 3.0% *6. strong sandstone*. All samples were saturated and, therefore, the void ratio e can be calculated from the water content w with the specific gravity G_s (Eq. (3)).

$$e = G_s \cdot w \tag{3}$$

The specific gravity of the marls is $G_s = 2.70$ and the specific gravity of the sandstones is assumed to be identical. Therefore, the void ratio for the marls ranges between $e = 0.14$ and 0.23, and for the sandstones between $e = 0.08$ and 0.21.

4.1. Unconfined compression tests

Unconfined compression tests (UCT) were carried out in undrained total stress conditions. Fig. 9 gives 6 examples of UCT tests, one for each rock unit. The overall results show that the sandstones are more brittle than the marls with the strength σ_{ci} increasing from *1. very weak marl* to *3. medium-weak marl* and from *4. soft sandstone* to *6. strong sandstone*, but with *3. medium-weak marls* being stronger than *4. soft sandstone*. The stiffness follows the same pattern and increases with strength.

Hoek et al. (2005) suggested an empirical first-estimate of the secant Young's modulus E_{50} with the UCT strength σ_{ci} (Eq. (4)).

$$E_{50} = \alpha \cdot \sigma_{ci} \tag{4}$$

where α is the stiffness coefficient and is a proxy for ductility.

The experimental data (Fig. 10) shows a good correlation between strength and stiffness for the marls with $\alpha = 90$, and a fair correlation with some scatter for the sandstones with $\alpha = 140$ for the *4. weak sandstone* and *5. medium-strong sandstone* and $\alpha = 240$ for the *6. strong sandstone*. These results show that the *red molasse* is more ductile than that in Greece and South-Africa where $\alpha = 300$ (Hoek et al., 2005).

4.2. Confined compression tests

Confined compression tests (CCT) were carried out in undrained total stress conditions with a 'Hoek' type apparatus for which the development of excess pore water pressure was not monitored. Therefore, the stresses are expressed as total stresses.

Fig. 11 gives 5 examples of CCT results, one for each rock unit; no confined compression tests were carried out for *6. strong sandstone*. The results show similar mechanical behaviours as for the UCT tests. The sandstones exhibit a stiff response to the loading (brittle) and the marls exhibit a more ductile behaviour. All specimens reach a peak state followed by a softening with the exception of *1. very weak marl*.

Fig. 12 shows the strength-stiffness relationship as defined in Eq. (5).

$$E_{50} = \beta \cdot q_f \tag{5}$$

where E_{50} is the secant Young's modulus, β the stiffness coefficient and $q_f = (\sigma_1 - \sigma_3)_f$ the deviatoric strength.

The results show that the marls have a stiffness coefficient $\beta = 40$ and the sandstone $\beta = 100$, with less scatter for the marls than for the sandstone. Post-test photographs of the specimens (Fig. 13) show the different failure modes – pure shear and mixed tensile-shear modes. *1. very weak marl* was totally destructured by the tests and *5. medium-strong sandstone* underwent a localised shear band failure.

Fig. 14 shows the stiffness of both CCT and UCT tests as a function on the initial void ratio. The results show that the stiffness increased as the void ratio decreased. *1. very weak marl* exhibit a very low stiffness and strength for a high void ratio, and *5. medium-strong sandstone* exhibited a high stiffness and strength for a low void ratios. *3. medium-weak marl* has a lower void ratio than the *4. weak sandstone* but exhibit a lower stiffness. Hoek et al. (2005) made similar observation when characterising the molasse in Greece.

4.3. Sonic wave velocity tests

Sonic wave velocity measurements were taken on the borehole core and shown in Fig. 4 and the mean values given in Table 1. Sonic wave velocities were also measured on laboratory specimens prior to testing and the results are shown in Fig. 15. The results show that a relationship between stiffness and sonic wave velocity exists with weaker rock having a lower velocity and stiffness than the stronger. However, a large range of velocities overlaps between the different rock sub-units, which makes the identification of the rock units difficult.

Table 1
Mechanical characteristics of the intact rock, after (GADZ, 2016a,b). Values are mean values with ± the standard deviation δ.

Variable	Units	Marls			Sandstones		
		1. Very weak	2. Weak	3. Med.-weak	4. Weak	5. Med.-strong	6. Strong[a]
w	[%]	8.6 ± 1.2	6.7 ± 1.2	5.0 ± 1.21	7.8 ± 1.8	4.1 ± 1.02	3.0 ± 1.09
ρ	[t/m^3]	2.44 ± 0.04	2.5 ± 0.04	2.55 ± 0.04	2.38 ± 0.06	2.56 ± 0.04	2.60 ± 0.03
w_L	[%]	51.4 ± 6.7	48 ± 5.5	(34.8 ± 3.7)	–	–	–
w_P	[%]	25 ± 2.6	23 ± 1.7	(20.7 ± 1.9)	–	–	–
σ_{ci}	[MPa]	3.7 ± 1.5	8.0 ± 2.87	15 ± 4.9	10.8 ± 3.2	22.9 ± 5.5	46.1 ± 14.2
E_s	[MPa]	340 ± 241	690 ± 534	1960 ± 1508	1230 ± 624	3420 ± 1490	9417 ± 4750
$\sigma_{ti,b}$	[MPa]	0.58 ± 0.31	1 ± 0.43	1.76 ± 0.7	0.8 ± 3.5	2.11 ± 0.77	3.3 ± 1.5
I_s	[MPa]	0.22 ± 0.13	0.33 ± 0.17	0.57 ± 0.27	0.26 ± 0.13	0.7 ± 0.27	1.59 ± 0.6
V_{pl}	[m/s]	2240 ± 425	2500 ± 444	3040 ± 536	2455 ± 456	3340 ± 547	3955 ± 524
RQD	[–]	71 ± 27	91 ± 13	97 ± 8	96 ± 8	98 ± 4	99 ± 2
ISRM grade		$R1$	$R2$	$R2$	$R2$	$R2$–$R3$	$R3$

Where w is the water content, ρ the unit density, w_L the liquid limit, w_P the plastic limit, σ_{ci} the intact rock unconfined compression strength, E_s the secant Young's modulus $\sigma_{ti,b}$ the Brazilian test tensile strength, I_s the point load test index and V_{pl} the longitudinal P-wave velocity. The ISRM grade (ISRM, 1981) are $R1$ for very weak rock (1 MPa $<\sigma_{ci}<$ 5 MPa), $R2$ for weak rock (5 MPa $<\sigma_{ci}<$ 25 MPa), and $R3$ for medium-strong (25 MPa $<\sigma_{ci}<$ 50 MPa).

[a] Inclusive of specimens containing limestone.

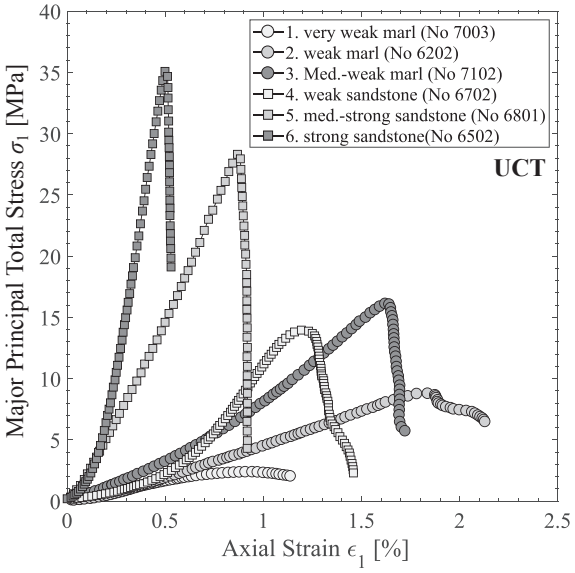

Fig. 9. Examples of unconfined compression tests for each rock unit.

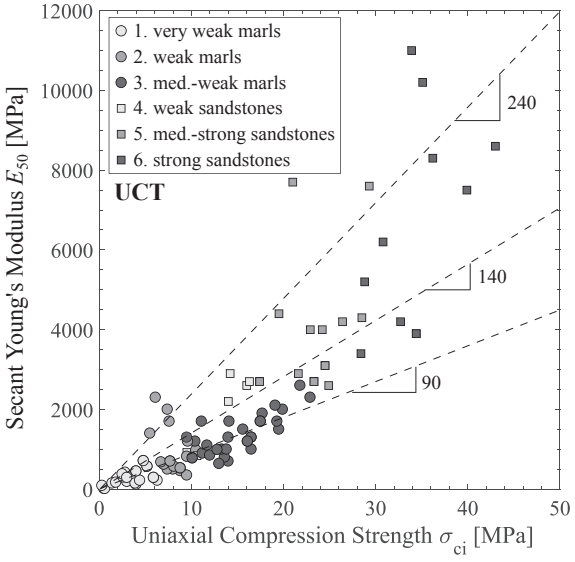

Fig. 10. Stiffness and strength of unconfined compression tests.

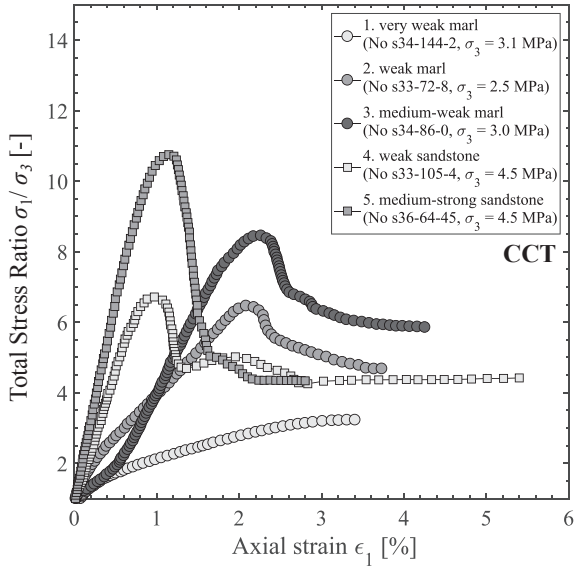

Fig. 11. Examples of confined compression tests for each rock unit, except *6. strong sandstone*.

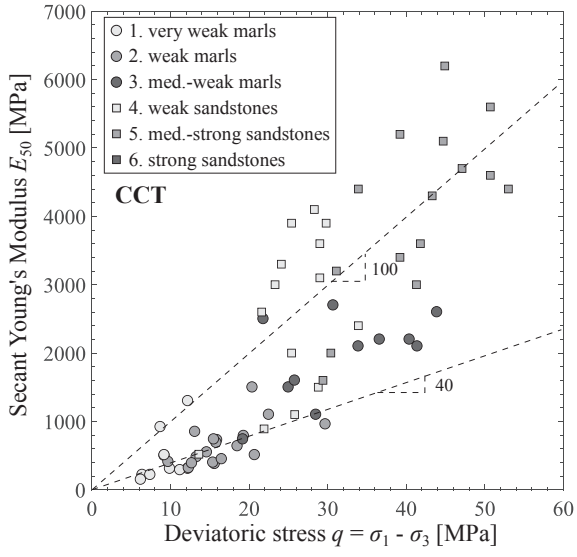

Fig. 12. Stiffness and strength of confined compression tests.

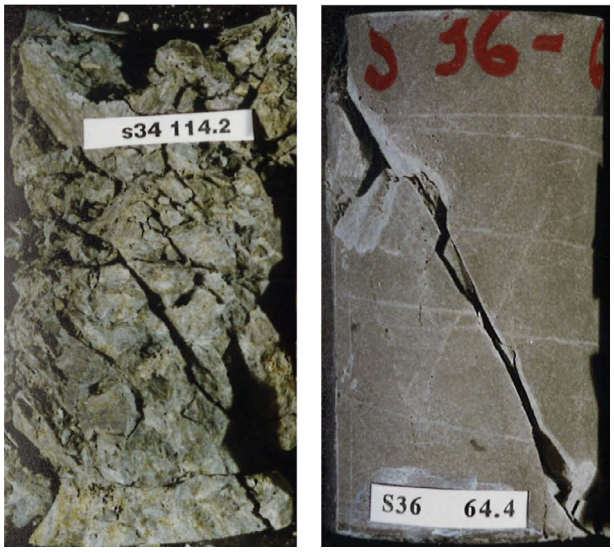

Fig. 13. Photographs of specimens after confined compression tests: *1. very weak marl* (left) σ_3 = 3.1 MPa and *5. medium-strong sandstone* σ_3 = 5.1 MPa (right).

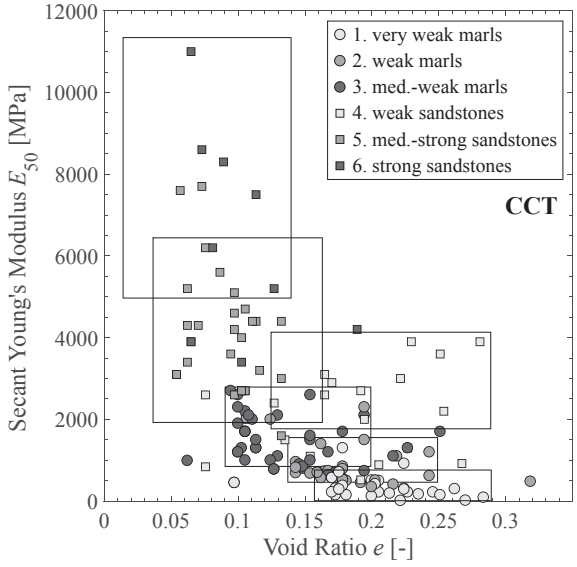

Fig. 14. Stiffness and initial void ratio of unconfined and confined compression tests.

4.4. Point load and Brazilian tests

Point load tests were systematically carried out. Fig. 4 gives the results for borehole C1 at Point 1 (ATLAS). The results show point load indices smaller than 1 MPa but can reach 2 MPa in other boreholes. Hoek (2007) does not recommend point load tests for weak rocks as it can lead to ambiguous results. Bieniawski (1989) excluded point load indices below 1 MPa from his rock mass classification system and favoured unconfined compressive strength instead; that is for rock grades *R*1 and *R*2. Point load tests are routinely done by geologist as a proxy for strength when documenting a borehole core. However, no attempt was made to correlate the point load index I_s with the strength of the intact rock.

The Brazilian test is also an indirect measurement of tensile strength. Fig. 16 shows the results of the Brazilian tests, which are comprised between 0 and 3 MPa, and a trend between the tensile strength and the void ratio; the tensile strength increases with the void ratio.

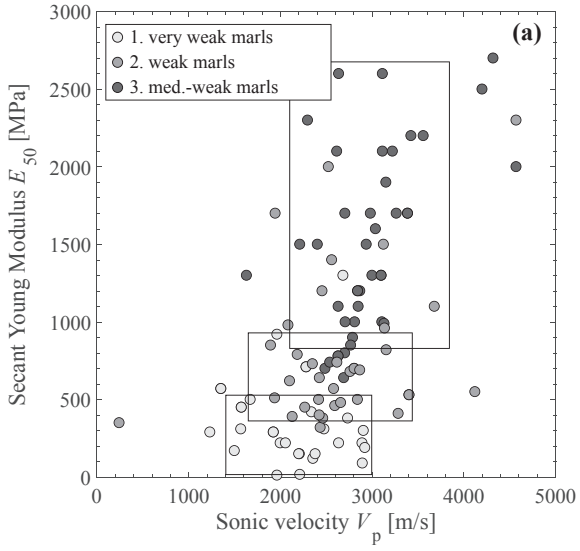

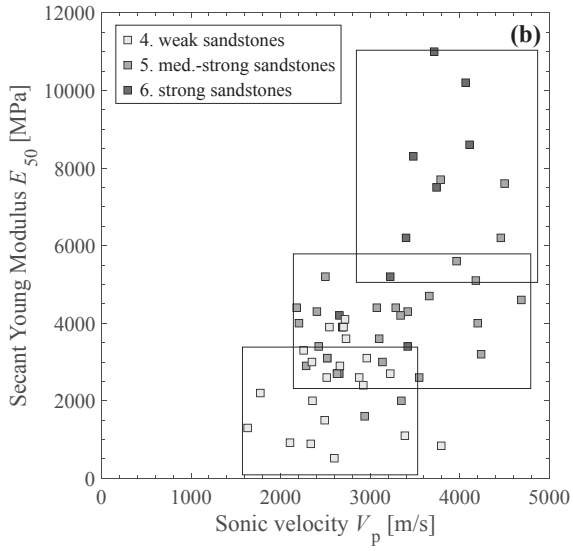

Fig. 15. Sonic wave velocity and stiffness of UCT and CCT of (a) marls and (b) sandstones.

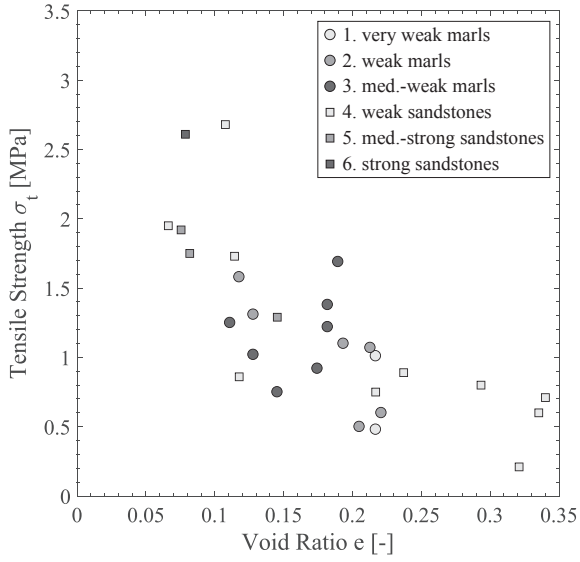

Fig. 16. Tensile strength from Brazilian tests versus the void ratio.

4.5. Discontinuities

Rock quality designation indices *RQD* (Deere, 1963) were calculated for each borehole. Fig. 4 shows values obtained for borehole C1 at Point 1 (ATLAS). The results show values in excess of 90 for the sandstones, but values as low as 0 can occur for some layers of *1. very weak marl*, *2. weak marl* and the weathered roof of the molasse. Table 1 gives the mean *RQD* values for the different rock units. The mean *RQD* of the sandstones is extremely high with a low standard deviation. *RQD* values for marls should be considered with caution. Hoek et al. (2005) made similar observation for the molasse in Greece and pointed out that the sandstone could be considered as intact rock.

A few apparent, but closed, joints were observed during the borehole logging. These occurred mainly in the marls and soft sandstones with a dip of 15° and 30° (GADZ, 2016a). Vertical and sub-verticals joints were also observed in the hard sandstones.

Direct shear tests were carried out on the discontinuities. The results suggest a friction angle of $\varphi = 12.7°$ and a cohesion of $c = 0.03$ MPa for *1. very weak marl* and $\varphi = 18°$ and $c = 0.015$ MPa for *2. weak marl* (GADZ, 1996). These values are lower than the residual strength of their respective intact rocks.

4.6. Swelling tests

Two series of swelling tests were carried out on intact marls – swell pressure tests and Huder-Amberg swell tests (Huder and Amberg, 1970). The swell pressure test consists in wetting the specimen in a confined environment (i.e. oedometer cell) with a fixed vertical pressure and to measure the vertical swell. Fig. 17 shows two examples of swell pressure test for *1. very weak marl* and *2. weak marl*, respectively. The results show that the magnitude of swelling is a function of the applied pressure, which counterbalances some of the swell. The results also show that the swell is approximately twice the magnitude for *1. very weak marl* than for *2. weak marl.*

The Huder-Amberg oedometer swell tests permit the determination of the swelling pressure with a single test. Fig. 18 shows three examples of tests for *1. very weak marl*, *2. weak marl* and *3. medium-weak marl*. The results show that the compression indices C_c increase from *1. very weak marl* to *3. medium-weak marl* but the swelling index C_s (unloading) is similar for all three groups of marls. However, marls are sensitive to sample disturbance (Einstein and Bischoff, 1975) and the given compression indices were not corrected. The specimens were subjected to wetting at a total vertical stress of $\sigma_v = 2$ MPa, which resulted in a contraction of the specimen for all three tests. However, the magnitude of contraction was more significant for *1. very weak marl* than for *2. weak marl* and very limited *3. medium-weak marl*. The swelling pressure corresponds to the intersection of the post-wetting unloading line and the initial compression line, and is 0.25 MPa for *1. very weak marl* and 0.1 MPa for *2. weak marl*. These pressures are consistent with the swell pressure tests for which the counterbalancing of the swelling was the most significant.

The results of the swelling tests show different swelling characteristics for the three groups of marls. The *1. very weak marl*, which are composed of high-plasticity clays, swelled more significantly than the *2. weak marl*, which are composed of medium–high plasticity clays, and the *3. medium-weak marl*, which are composed of low-plasticity clays. Huder and Amberg (1970) also observed significant differences in swelling characteristics of other Swiss marls. Einstein and Bischoff (1975) pointed out that the swelling characteristics of marls were largely due to the clay minerals and that the swelling is more significant for fresh water deposited marls than for salt water deposited marls.

4.7. Permeability tests

Permeability tests were carried for the intact rock and gave values in the range of 10^{-10}–10^{-11} m/s but the rock units were not specified

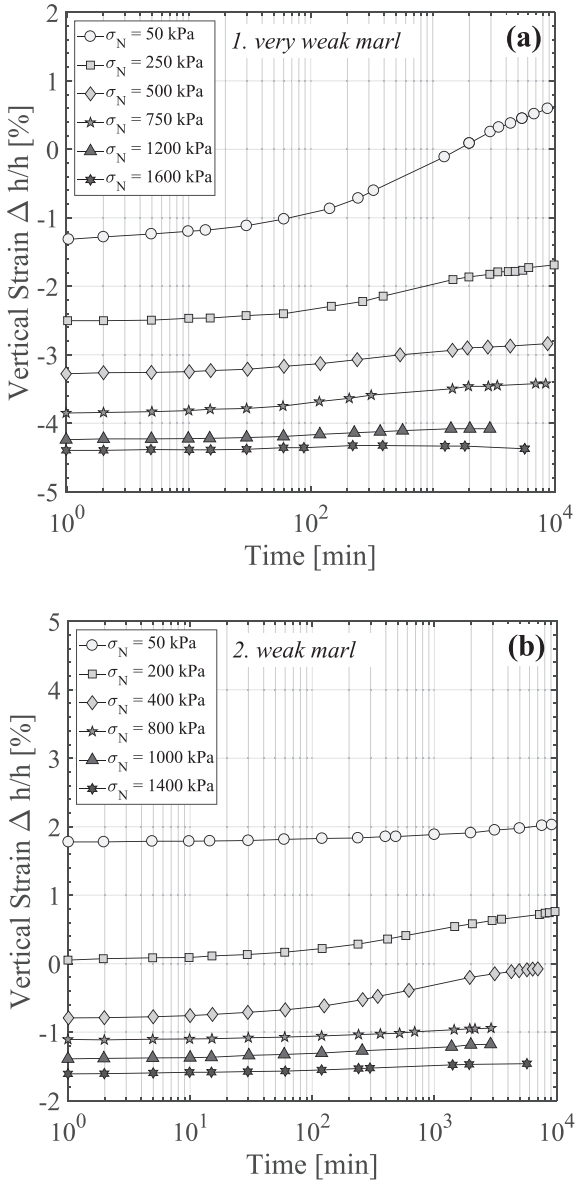

Fig. 17. Swelling tests in oedometer cell for (a) *1. very weak marls* and (b) *2. weak marls*.

(CERN, 1972). The average permeability was also calculated by measuring the ingress of water in the boreholes and suggested a permeability of the rock mass of 10^{-9} m/s (CERN, 1972). The difference in permeability was attributed to fractures in the rock mass. However, one anomaly was found in borehole F1 at a depth of 56.6 to 66.4 m with a permeability of 10^{-5} m/s (CERN, 1972).

Lugeon tests were carried out in boreholes at Point 1 (ATLAS) and Point 5 (CMS). The test consisted of putting the water in borehole under a pressure of 1 MPa at Point 1 and 0.75 MPa at Point 5 and to monitor the rate of water loss. The results showed little water loss, suggesting a very low permeability of the molasse (GADZ, 2016a,b); the loss of water was lower than the accuracy of the instruments. These tests were carried out deeper than the underground structures at CERN and in zones with very few discontinuities (Fig. 4).

The molasse is known to have a very low permeability. However, 13 water ingresses were observed during the 27 km excavation of the LEP/LHC tunnel with maximum inflow of 120 l/min (6 l/min/km). These water ingresses were located between Point 7 and Point 8, and suggested a permeability as low as 10^{-9}–10^{-10} m/s (≈0.01 Lugeon) (GADZ, 2016a).

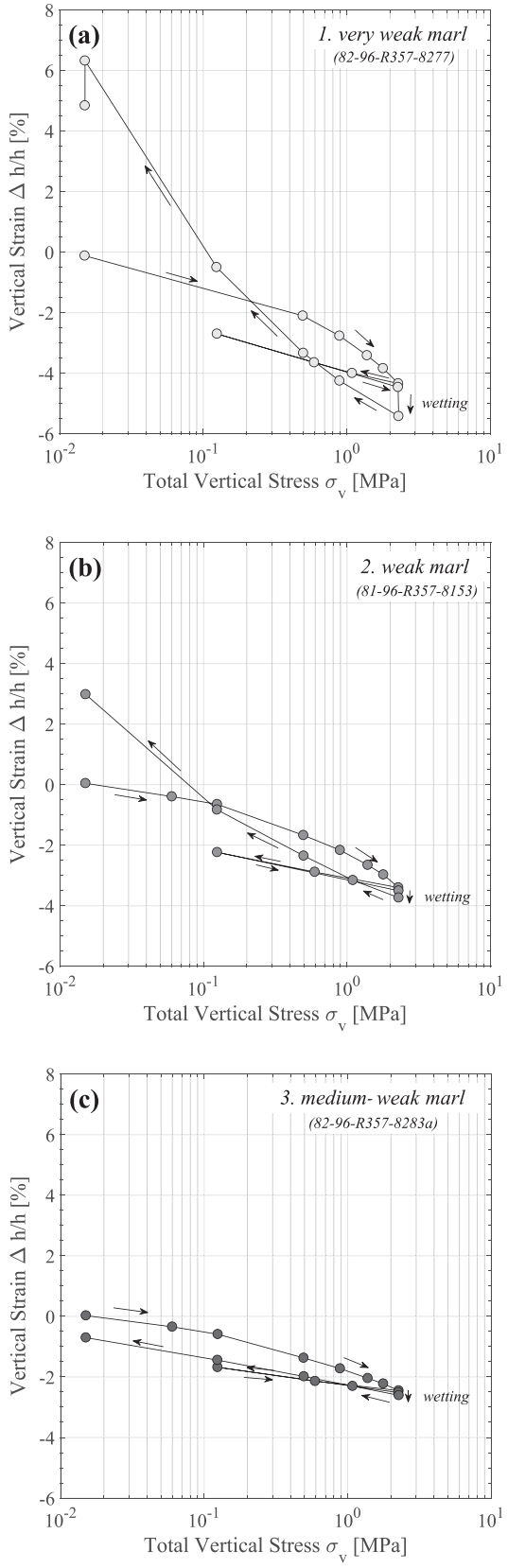

Fig. 18. Huder-Amberg swelling tests for (a) *1. very weak marl*, (b) *2. weak marl* and (c) *3. medium-weak marl*.

5. Strength envelopes

The peak and residual total stress states of the UCT and CCT tests are summarized in Fig. 19, in which σ_3 is the initial total confining pressure. The zones of the different failure modes are also plotted as discussed by Hoek and Martin (2014). A Hoek-Brown (HB) failure criterion (Hoek and Brown, 1980), given in Eq. (6), is fitted to each rock unit. However, it is also possible to fit other failure criteria to the data such as a pressure-dependent Tresca criterion.

$$\sigma_{1,f} = \sigma_{3,0} + (m_i \cdot \sigma_{3,0} \cdot \sigma_{ci} + s \cdot \sigma_{ci})^a \quad (6)$$

where $\sigma_{1,f}$ is the major principal total stress at failure, $\sigma_{3,0}$ is the minor principal total stress, σ_{ci} the unconfined compression strength of intact rock, m_i the HB material constant which is typically $m_i = 7 \pm 2$ for marls and $m_i = 17 \pm 4$ for sandstones (Hoek and Brown, 1997), s a model parameters which is $s = 1$ for intact rock and $s = 0$ for crushed/jointed rock, and a another model parameter which is typical $a = 0.5$ for intact rock.

The HB failure criterion predicts the total stress failure envelope from the UCT strength σ_{ci} and a material parameter m_i and two model parameter a and s. The UCT strengths σ_{ci} given in Table 1 were used for all rock units except *6. strong sandstone*, for which the unconfined strength σ_{ci} was reduced to fit the data. This is because some very strong sandstones containing lime were included in Table 1. The 'mean' failure envelope is plotted with a continuous line, and the 'minimum' and 'maximum' envelopes with a dashed line. The a parameter controls the curvature of the envelope and has a default value of $a = 0.5$ for intact rock at peak state (Hoek and Brown, 1980; Hoek, 1983). However, it is lowered in a few cases for the residual state in order to fit the data. The s parameter controls the tensile strength and has a default value at peak state of $s = 1.0$. It is set to $s = 0$ for the residual state as it is assumed that the rock was destroyed and had no tensile strength. The m_i parameter is then curve-fitted such that the failure envelope fitted both the peak and residual states of the CCT tests.

The UCT strength data is then used to verify the position of the peak failure envelope ($\sigma_1 = \sigma_{ci}$, $\sigma_3 = 0$). The tensile strength obtained from the Brazilian tests is used to compare the position of the envelope ($\sigma_1 = 0$, $\sigma_3 = -\sigma_{ti,b}$) with the experimental data.

Fig. 19(a) shows the experimental data for *1. very weak marl* alongside the HB failure envelopes. The data shows that the peak state is very similar to the residual state and, hence, no softening phase takes place. However, a small difference in the tensile strength is observed. Both the peak and residual HB failure envelopes follow the data with a material parameter $m_i = 4$. This value is very low even for marls. The HB parameters are found to be $s = 0$, which relates to crushed/blocky rocks, and $a = 0.5$ at peak state and $a = 0.48$ at residual state.

Fig. 19(b) shows the experimental data for *2. weak marl* alongside the HB failure envelopes. Unlike for *1. very weak marl*, a small difference between the peak and residual states is observed. The HB failure envelopes are fitted to the data and the material parameter is found to be $m_i = 10$, which is fairly high for marls (Hoek and Brown, 1997) and contrasts with *1. very weak marl*. The two other HB parameters are found to be ($a = 0.5$, $s = 1$) and ($a = 0.43$, $s = 0$) for the peak and residual states, respectively.

Fig. 19(c) shows the experimental data for *3. medium-weak marl* alongside the HB failure envelopes. The data shows a substantial difference between the peak and the residual states suggesting an important softening phase. The HB material parameter is found to be $m_i = 15$. This is a high value for marls but standard for sandstone. However, the stress-strain curves show that the stiffness of *3. medium-weak marl* is lower than those of sandstones. The two other HB parameters are found to be ($a = 0.5$, $s = 1$) and ($a = 0.425$, $s = 0$) for the peak and residual states, respectively.

Fig. 19(d) shows the experimental data for *4. weak sandstone* alongside the HB failure envelopes. The results confirm its lower strength in comparison to *medium-weak marl*. The material parameter is

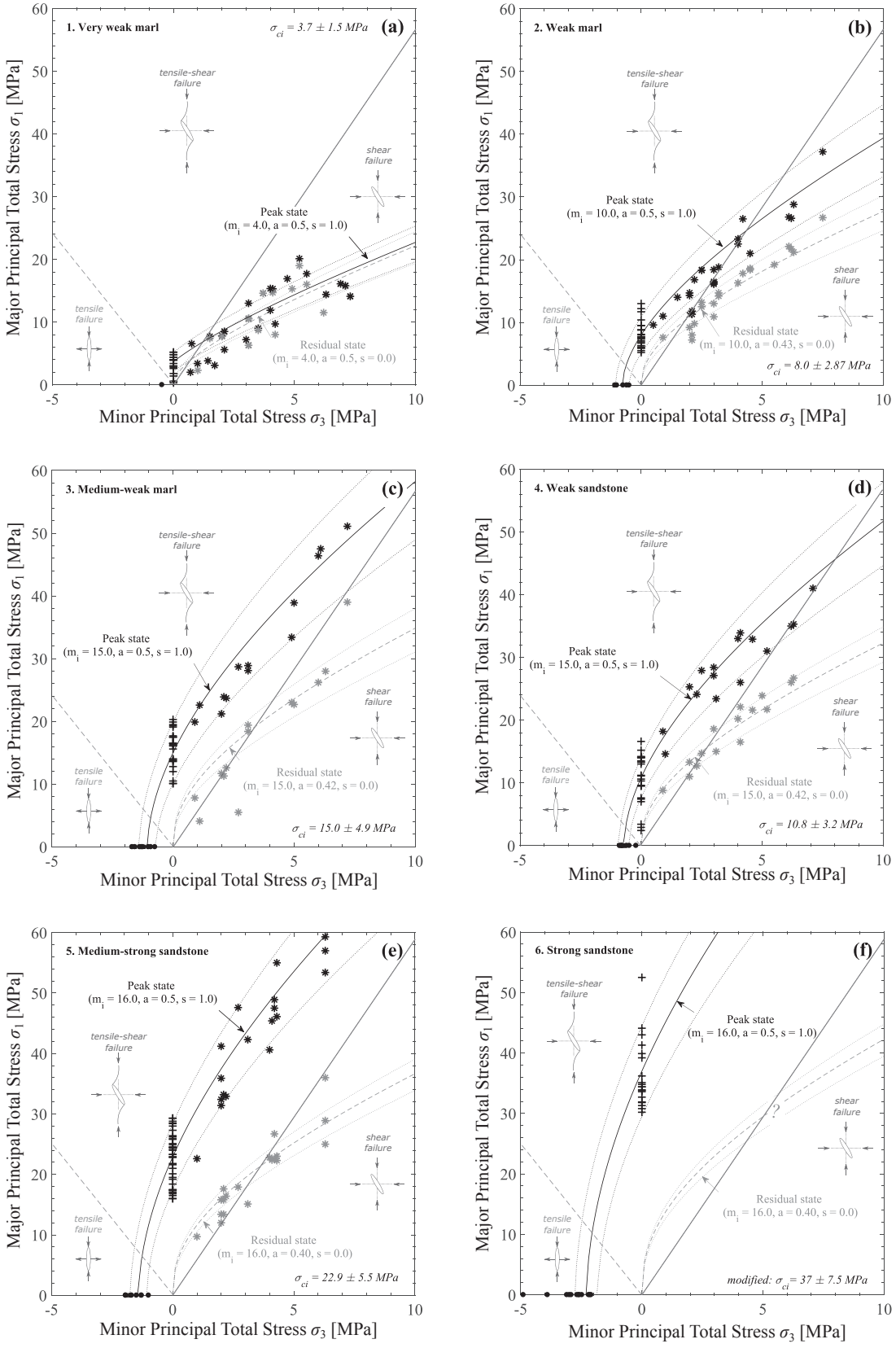

Fig. 19. Total stress Hoek-Brown failure envelope based on unconfined compression, confined compression and Brazilian tests.

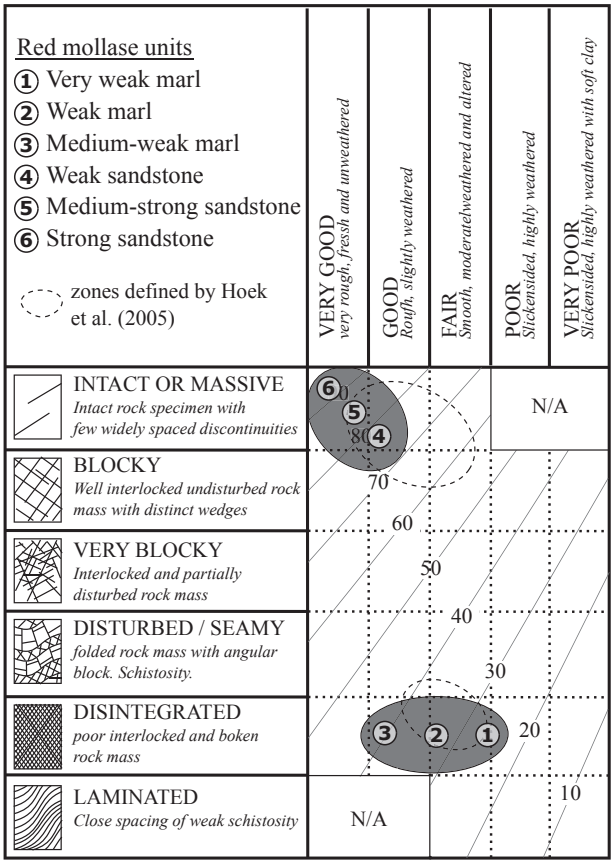

Fig. 20. GSI determination of the red molasse units at CERN. Shaded zones are for the *red molasse* and dashed-line zones are for Greek molasse (Hoek et al., 2005).

found to be $m_i = 15$ and is the same as for *3. medium-weak marl*. However, the UCT strength is smaller and the failure envelopes are hence lower. Nevertheless, the same material parameter m_i highlights the similarity between both rock units. The two other model parameters are ($a = 0.50$, $s = 1.0$) and ($a = 0.42$, $s = 0$) for the peak and residual states, respectively.

Fig. 19(e) shows the experimental data for *5. medium-strong sandstone* alongside the HB failure envelopes. The material parameter is found to be $m_i = 16.0$, a typical value for sandstones. The two other model parameters are ($a = 0.5$, $s = 1$) and ($a = 0.42$, $s = 0$) for the peak and residual states, respectively.

Fig. 19(f) shows the experimental data for *6. strong sandstone* alongside the peak HB failure envelope. Due to the absence of CCT tests, the HB parameters are assumed to be identical to *5. medium-strong sandstone* with $m_i = 16.0$, $a = 0.5$ and $s = 1$.

It is well recognised the failure of intact rock is related to the propagation of cracks within the medium (i.e. Griffith, 1921). At low confining pressures, tensile fracturing initiates in specimens with confining pressures in the order of 40–60% of the unconfined compressive strength ($\sigma_{3,0} = 0.40–0.60 \cdot \sigma_{ci}$) (Hoek and Martin, 2014). The results show that *1. very weak marl* fails in a pure shear failure mode and it would be more appropriate to characterise this rock unit in an effective stress framework. However, pore pressures were unavailable and, hence, the effective stress are unknown. All others failed in a mixed tensile-shear mode, typical of rocks.

5.1. Geological strength index

It is customary to derive the model parameters for fractured rock masses from the intact rock model parameters with an index called the geological strength index (*GSI*) (Hoek, 1994). The *GSI* aims to quantify the level of fracturation and quality of the joints, which influences the rock mass strength. Marinos and Hoek (2001) suggested that the *GSI* values for sandstone were comprised between 45 and 90, depending on the state of weathering, and argued that the *GSI* is not applicable for marls. Hoek et al. (2005) provided an extensive discussion on the use of the *GSI* for the molasse in Greece. They pointed out that the sandstone units were poorly fractured and would have a *GSI* value close to 100 (unweathered). Hence, the mechanical behaviour of the rock mass would apparent itself to the intact rock. Hoek et al. (2005) and Marinos et al. (2005) suggested that the *GSI* values for the marls would be in the range of 30–40 as these rocks are micro-fissured, and close to 100 (unweathered) for the sandstones. Fig. 20 show suggested zones for the sandstones and the marls at CERN, for which the *GSI* of the marls covers a wider region and is 100 for the sandstone.

6. Conclusion

This paper presented a geotechnical characterisation of a weak sedimentary rock at CERN, Geneva. It is based on extensive data gathered in the past 70 years by CERN and consisted of exploration boreholes, laboratory tests and *in situ* tests. Although only a summary of the tests is presented in this paper, the results show the general characteristics of a weak sedimentary rock called the *red molasse*. This rock mass is composed of two rock units – marls and sandstones – and three sub-units exist for each rock unit. These sub-units form lenses in the bedrock with smooth transition between them making any prediction difficult. The rock mass is generally massive and can be viewed as a continuum solid. However, local fractured zones are observed and are mostly in very weak layers of marl and can be treated as a soil-like rock unit.

The marls result from the diagenesis of clayey-silty Alpine detritus, and the sandstone of silty-sandy Alpine detritus. The strengths of the marls ranged from *very weak* (*R*1) to *weak* (*R*2). It was found that *1. very weak marl* are composed of high-plasticity clays, *2. weak marl* of medium-high plasticity clay and *3.medium-weak marl* of low-plasticity clays. The strength of the sandstone ranges from *weak* (*R*2) to medium-strong (*R*3) and relates to the grain size and their clay content. An overlap of strength is observed between the stronger marls and the weaker sandstones but has a different stiffness; the marls are found to be ductile and the sandstone more brittle. This difference is not captured by the International Rock Classification System, which is based on strength only. The *1. very weak marl* were found to be significantly weaker compared to other units and are subject to slaking and swelling. It was also shown that the *red molasse* was more ductile than the molasse in Greece and South Africa.

Acknowledgements

This project has received funding from the Swiss National Science Foundation under grant agreement P2SKP2 171774 and support from the European Organisation for Nuclear Research (CERN). The authors would like to thank Mr. Laurent Gastaldo for retrieving the laboratory data from the archives of the Swiss Federal Institute of Technology of Lausanne (EPFL).

References

Barton, N., 2007. Rock Quality, Seismic Velocity, Attenuation and Anisotropy. Francis & Taylor, London ISBN 9780415394413.
Bieniawski, Z.T., 1989. Engineering Rock ASS Classification. Wiley Interscience, New York.
CERN, 1972. The 300 GeV Programme. CERN, Geneva.
Deere, D.U., 1963. Technical description of rock cores for engineering purposes. Felsmechanik Ingenieurgeologie (Rock Mech. Eng. Geol.) 1 (1), 16–22.
Einstein, H., Bischoff, N., 1975. Design of tunnels in swelling rock. In: 16th US Symposium on Rock Mechanics, Minneapolis. American Rock Mechanics Association, pp. 22–24.
GADZ, 1996. Reconnaissances géologiques et géotechniques – rapport d'interprétation No

3545/91. Technical report, Géotechnique Appliquée Dériaz SA, Geneva (in French).
GADZ, 1997. Reconnaissances de la Molasse – Rapport de Synthèse – No 3545.97. Technical report, Géotechnique Appliquée Dériaz Ltd, Geneva (in French).
GADZ, 2016a. Reconnaissances géotechnique Point 1 – No 7222/2. Technical report, Géotechnique Appliquée Dériaz SA (in French).
GADZ, 2016b. Reconnaissances géotechniques – No 7223/2. Technical report, Géotechnique Appliquée Dériaz SA (in French).
Griffith, A.A., 1921. The Phenomena of Rupture and Flow in Solids. Philos. Trans. Roy. Soc. A: Math. Phys. Eng. Sci. 221 (582–593), 163–198. http://dx.doi.org/10.1098/rsta.1921.0006. ISSN 1364-503X.
Heidbach, O., Rajabi, M., Reiter, K., Ziegler, M., 2016. World Stress Map Database Release 2016. GFZ Data Services. http://dx.doi.org/10.5880/WSM.2016.001. URL < http://www.world-stress-map.org > .
Hoek, E., 1983. Strength of jointed rock masses. Géotechnique 23 (3), 187–223.
Hoek, E., 1994. Strength of rock and rock masses. ISRM News J. 2 (2), 4–16.
Hoek, E., 2007. Practical rock engineering. Rocscience.
Hoek, E., Brown, E.T., 1980. Empirical strength criterion for rock masses. J. Geotech. Eng. Div. 106 (GT9), 1013–1035.
Hoek, E., Brown, E.T., 1997. Practical estimates of rock mass strength. Int. J. Rock Mech. Min. Sci.1 43 (8), 1165–1186.
Hoek, E., Martin, C.D., 2014. Fracture initiation and propagation in intact rock – a review. J. Rock Mech. Geotech. Eng. 6 (4), 287–300. http://dx.doi.org/10.1016/j.jrmge.2014.06.001. ISSN 16747755.
Hoek, E., Marinos, P.G., Marinos, V.P., 2005. Characterisation and engineering properties of tectonically undisturbed but lithologically varied sedimentary rock masses. Int. J. Rock Mech. Min. Sci. 42 (2), 277–285. http://dx.doi.org/10.1016/j.ijrmms.2004.09.015. ISSN 13651609.
Huder, J., Amberg, G., 1970. Quellung in Mergel, Opaliuston und Anhydrit. Schweizer Bauzeitung 43, 975–980. http://dx.doi.org/10.5169/seals-84648. (in German).
ISRM, 1981. Rock Characterisation, Testing and Monitoring. Technical Report, International Society of Rock Mechanics, Oxford.
Laughton, C.. 1990. Rock support of the L3 experimental hall complex. In: Unique Underground Structures Symposium, Denver.
Lombardi, G., 1979. Rock mechanics at the CERN proton-antiproton facilities. In: Internation Society for Rock Mechanics (Ed.), 4th ISRM Congress. International Society for Rock Mechanics, Montreux. Balkema, pp. 433–436.
Lombardi, G., 1981. Les ouvrages souterrains du CERN. Publication de la Société Suisse de Mécanique des Sols et des Roches 104, 47–53 (in French).
Marinos, P.G., Hoek, E., 2001. Estimating the geotechnical properties of rock masses such as flysch. Bull. Eng. Geol. Environ. 60, 85–92.
Marinos, V., Marinos, P.G., Hoek, E., 2005. The geological strength index: applications and limitations. Bull. Eng. Geol. Environ. 64 (1), 55–65. http://dx.doi.org/10.1007/s10064-004-0270-5. ISSN 14359529.
Marinos, V., Prountzopoulos, G., Fortsakis, P., 2013. Tunnel behaviour and support in molassic rocks. experience from 12 tunnels in Greece. In: Kwasniewski, M., Lydzba, D. (Eds.), Rock Mechanics for Resources, Energy and Environment, 909–914. CRC Press, London. ISBN: 9781138000803. http://dx.doi.org/10.1201/b15683-156.
Sloan, A., Moy, D., Kifger, D., 1996. 3D modelling for underground excavation at point 1, CERN. In: Eurock'96. Balkema, pp. 957–963.
Swiss Geological Survey, 2013. Geology of Switzerland – Knowledge from the Underground. ISBN 9783302400716.